Integrated Aerodynamic-Structural Design of a Subsonic, Forward-Swept Transport Wing

by

David M. Polen

Thesis submitted to the Faculty of the

Virginia Polytechnic Institute and State University

in partial fulfillment of the requirements for the degree of

Master of Science

in

Aerospace Engineering

APPROVED:

Dr. B. Grossman, Chairman

Dr. R. T. Haftka

Dr. J. A. Schetz

April 1989

Blacksburg, Virginia

Integrated Aerodynamic-Structural Design of a Subsonic, Forward-Swept Transport Wing

by

David M. Polen

Dr. B. Grossman, Chairman

Aerospace Engineering

(ABSTRACT)

The introduction of composite materials and the ability to tailor these materials to improve aerodynamic and structural performance is having a distinct effect upon aircraft design. In order to optimize the efficiency of the design procedure, a design process which is more integrated than the traditional approach is required. Currently the utilization of such design procedures produces enormous computational costs. An ongoing effort to reduce these costs is the development of efficient methods for cross-disciplinary sensitivities and approximate optimization techniques.

The present research concentrates on investigating the integrated design optimization of a subsonic, forward-swept transport wing. A modular sensitivity approach for calculating the cross-sensitivity derivatives is employed. These derivatives are then used to guide the optimization process. The optimization process employed is an approximate technique due to the complexity of the analysis procedures. These optimization results are presented and the impact of the modular technique is discussed.

Acknowledgements

I would like to thank Dr. Bernard Grossman and Dr. Rafael Haftka for their insight and guidance during the course of my research. Their patience and ability to provide proper direction allowed for a very educational and enjoyable working relationship. I am honored to have been able to study under them.

I would also like to thank Dr. Pi-Jen Kao and for their supporting efforts in the structural and performance analyses for the project. I would like to thank for his help in preparing this thesis.

I would especially like to thank my mother and father whose hard work and unyielding faith made it possible for me to pursue my academic dreams. I dedicate this thesis to them.

Table of Contents

List of Illustrations

List of Tables

Nomenclature

A	Aerodynamic influence coefficient matrix
A'	Derivative of A matrix
$b/2$	Wing half-span
C_L	Coefficient of lift
C_ℓ	Section lift coefficient
$C_{Df,t}$	Drag coefficient for fuselage and tail
$C_{D_{a/c}}$	Drag coefficient for reference aircraft
$C_{D_{i0}}$	Coefficient of induced drag at $\alpha = 0$
$C_{D_{v0}}$	Coefficient of viscous drag at $\alpha = 0$
$\vec{C}_{m,n}$	Influence coefficient vector at point m induced by Γ_n
c'	Thrust specific fuel consumption
C_p	Pressure coefficient (compressible)
C'_p	Pressure coefficient (incompressible)
C_D	Drag coefficient
C'_D	Drag coefficient (incompressible)
C'_L	Lift coefficient (incompressible)
D_i	Induced drag on ith panel
D_m	Drag at optimum altitude
D	Drag
F_{ar}	Rigid wing vertical forces at load set nodes
$\vec{F}_i$	Force vector on panel i
F_a	Vertical forces at load set nodes
F_z	Vertical aerodynamic forces

F_I	Gravitational and inertial load forces
g_s	Design constraints
J	Jacobian matrix
L_i	Lift on ith panel
L_s	Section lift force
L	Lift
M_∞	Freestream Mach number
NTP	Number of aerodynamic panels
NDV	Number of design variables
n	Load factor
p	Design parameters (also design variables)
q	Dynamic pressure
q_D	Divergence dynamic pressure
q_m	Dynamic pressure at optimum altitude
R	Incremental aerodynamic force vector
R_g	Calculated range
R_{ref}	Reference aircraft range
S_w	Wing area
S_s	Wing section area
S'	Derivative of S matrix with respect to p
S	Flexibility matrix
T	Boolean transformation matrix
U	Displacement vector
U_∞	Freestream velocity
$\vec{V}_{m,n}$	Velocity vector at point m induced by Γ_n
$\vec{V}$	Velocity vector (induced + freestream)
$\vec{V}_{ind}$	Induced velocity vector
$\vec{V}_i$	Velocity vector on panel i
V_s	Wing volume
V_{ref}	Reference aircraft wing volume
V_c	Cruise velocity
W_s	Aircraft standard empty weight
W_{UF}	Usable fuel weight
W_G	Gross weight
W_S	Aircraft standard empty weight
W_P	Payload weight

W_{RS}	Reference aircraft standard empty weight
W_{RW}	Reference aircraft wing weight
W_W	Wing weight
W_0	Design weight
x,y,z	Compressible coordinates
x′, y′, z′	Incompressible coordinates
α	Angle of attack
α_r	Rigid angle of attack
Γ	Vortex strength
$\vec{\Gamma}_i$	Vorticity vector on ith panel
ϕ	Slope of mean camber surface in x-z plane
ψ	Slope of mean camber surface in y-z plane
ρ	Freestream density
θ	Structural vertical displacements
η	Structural weight savings factor
$\vec{\Phi}$	Velocity potential vector
Φ	Velocity potential (compressible regime)
Φ'	Velocity potential (incompressible regime)

1.0 Introduction

At the heart of any integrated engineering design problem is the need for effective coordination and communication between the various engineering disciplines involved. Traditionally these different disciplines interact mainly during the preliminary design phase or in crisis situations. Until recently, aircraft design procedures were for the most part performed in a sequential manner. The aerodynamicist would first design a wing for optimum shape. The structural analysts would then design an internal structure for minimum weight. Now however, the versatility of composite materials requires the integration of the different disciplines throughout the design process. Composite materials can be tailored to improve the aerodynamic and structural performance of an aircraft giving rise to the need for an integrated multi-disciplinary design process. For example, consider the Grumman X-29A forward-swept-wing fighter. Because a metal wing has a destabilizing bending-twisting coupling, composite materials were used and tailored to produce favorable bending-twisting coupling. The use of composite materials to control the aeroelastic response of and improve the performance of an aircraft is known as aeroelastic tailoring. Using this in conjunction with an integrated

aerodynamic-structural design process provides aircraft designers with a powerful tool which can be used for controlling aeroelastic phenomena such as flutter and wing divergence (Ref. 1 and 2).

Integration in the traditional design approach was limited primarily due to the nature of the metal materials used and the enormous computational costs associated with integrated design. These costs arise from the sophisticated models used by the structural and aerodynamic analysts. For the integrated design method to be practical, efficient methods for cross-disciplinary sensitivities and optimization procedures are necessary.

Past research at this university, focused on the integrated design of a high aspect ratio sailplane wing. The sailplane mission of circling flight in a thermal followed by cross-country cruise was used to illustrate the advantages of the integrated design process. The use of the simple analysis methods of lifting-line theory for the aerodynamics and beam theory for the structural analysis made it feasible to calculate all of the aerodynamic and structural sensitivity derivatives directly at each step of the optimization process. The results of this work demonstrated that the integrated design process produces wing designs superior to those obtained by the traditional sequential design approach (Ref. 3).

The next step of the integrated wing design study still used the sailplane as a model but employed analysis methods which are more representative of design methods used for low speed aircraft wing design. The use of the vortex-lattice method for the aerodynamic analysis and a structural finite-element method introduced complexities involving the need for more independent design variables and constraints, and were substantially more expensive than previous design procedures. By incorporating perturbation methods for cross-sensitivity derivatives

and using approximate optimization techniques, an estimated 10 hours of IBM 3090 CPU time was reduced to less than 10 minutes (Ref. 4).

The present research is part of the ongoing integrated wing design project and focuses on a forward-swept wing for a subsonic transport aircraft. The vortex-lattice method and a structural finite-element method are still considered. However, the use of an aeroelastic analysis which is more refined than that which was employed in the sailplane design produces additional computational costs. The reduction of these costs is pursued using

1. efficient methods for cross-sensitivity calculation ; and
2. approximate optimization techniques.

The sensitivity calculation is based on a modular sensitivity method (Ref. 5). Using this approach, the system is divided into a sequence of interacting "black boxes" each of which represents a specific design discipline. Decomposition of the system into a multilevel approach preserves discipline independence for the system optimization problem (Ref. 6). The modular approach allows for the calculation of sensitivity derivatives with a higher accuracy and generally, at a lower cost than finite differencing. The system sensitivities are used to guide an optimization and a Newton's method solution of the coupled interdisciplinary equations describing the system. Also, using the modular approach, the aeroelastic sensitivities can be computed without the expensive calculations of the derivatives of the aerodynamic influence coefficient matrix and the flexibility matrix. The calculation of these derivatives represents a substantial amount of the computational costs associated with the integrated design process in reference 4.

The objective of this research is to investigate the use of a modular sensitivity analysis method to effectively and efficiently calculate cross-disciplinary sensitivities used to guide an approximate optimization procedure. A sufficient number of wing design parameters has been chosen to provide an accurate investigation of the modular sensitivity approach. However, the use of these relatively few design parameters yields simplified optimization results.

Chapter 2 presents the aerodynamic and structural models and a discussion of the aerodynamic analysis method used for the wing design. The aeroelastic analysis/sensitivity method is given in Chapter 3. Chapter 4 outlines the wing optimization process and presents a discussion of the design results. Finally, concluding remarks about the analysis method are presented in Chapter 5.

2.0 Forward-Swept Wing Transport

A forward-swept wing is chosen for the integrated design study in order to fully utilize the strong aerodynamic/structural interactions associated with this type of wing to guide the design process. The choice of a forward-swept wing also provides favorable conditions for using a natural laminar flow airfoil. In addition, because of the increased complexity of the analysis for transonic flow, subsonic flow with Mach number of about 0.5 is chosen as the design condition.

The mission of the forward-swept wing transport consists of two flight conditions. The first is constant altitude cruise and the aerodynamic performance is based on this portion of the the mission. The second phase of the mission is a 2.5g pull-up maneuver. The analysis during the maneuver is performed to evaluate the design constraints of maximum stress and strain imposed on the wing structure and the wing divergence constraint.

The design objective is to minimize the gross weight of the aircraft. This is pursued by reducing the wing weight which allows for weight reductions in other structural components. The reduced structural weight of the aircraft can then be used for increasing the aircraft's range or payload capacity.

2.1 Aerodynamic Model

The planform of the forward-swept transport wing is shown in figure 1. The six design parameters represent the planform design variables. Two other aerodynamic design variables are the twist angles at the break and tip. The twist schedule of the wing is modeled linearly continuous from root to tip. The airfoil section, for all spanwise stations, is a natural laminar flow airfoil designated as the HSNLF(1)-0213 described in reference 7 and shown in figure 2. The airfoil is designed for a Mach number of 0.7 and a lift coefficient of 0.2. Substantial wind tunnel test data is presented in reference 7. The aerodynamic analysis for the wing is based on the vortex-lattice method discussed in section 2.3. A total of 120 aerodynamic panels (12 spanwise, 10 chordwise) are used to model the wing. The 120 panel scheme has proven to provide suitable accuracy at reasonable computational cost.

2.2 Structural Model

The finite element model of the forward-swept transport wing is shown in figure 3. The model has 534 degrees of freedom and 1093 elements. There are 684 anisotropic triangular membrane elements to model the graphite/epoxy wing skins which are stacked up of 0°, ± 45°, and 90° plies with the 0° direction being a design variable. 138 shear web elements model the spar webs. The remaining elements are truss elements which model the spar caps, the vertical stiffness of the ribs and spars, and provide a crude model of the leading/trailing edge structure. The leading

and trailing edge truss elements are used for transferring the aerodynamic loads to the wing box. A more detailed discussion of the wing structure is given in reference 8.

2.3 Aerodynamic Formulation

The vortex-lattice method is a panel method used to compute the forces on a thin swept wing assuming steady, inviscid, irrotational, and incompressible flow. The continuous distribution of vorticity on the wing is modeled by a distinct number of discrete horseshoe vortices located on a finite number of panels into which the wing is divided. The strengths of these individual vortices determine the forces acting on each panel. Ultimately, the total lift, drag and their corresponding coefficients may be found.

On the wing there is a spanwise distribution in the lift force. As a result of this distribution air on the upper surface of the wing flows inward toward the root. Similarly, air on the lower surface flows outward toward the tip. The differences between the spanwise velocity components on the upper and lower surfaces of the wing will cause the air to roll up into small vortices distributed spanwise at the trailing edge. These small vortices roll up into two large vortices at the wing tips. At this point it is customary to make two assumptions. First that these vortices form an infinitesimally thin surface of discontinuity known as the vortex sheet; and second that this sheet remains flat and extends downstream to infinity parallel to the x-axis.

Since the wing is of small lateral thickness, the vortex lattice panels are located on the mean camber surface. Thus, the vortices may be considered to be bound to

the wing along the mean camber surface and when they leave the wing, they generally follow a curved path. Consistent with the usual thin wing assumptions employed in the vortex-lattice method, suitable accuracy can be obtained assuming straight-line trailing vortices. Applying the flow tangency boundary condition at each panel results in a system of equations which may be solved for the unknown individual vortex strengths. Each panel has associated with it a control point at which the flow tangency boundary condition is applied. Following the development in Bertin and Smith (Ref. 9), the vortex is bound at the quarter-chord location of the panel and the control point is located at the three-quarter-chord location as shown in figure 4.

The velocity induced at a point by a vortex filament of strength Γ and a length $d\ell$ is given by the Biot-Savart law as

$$d\vec{V} = \Gamma \frac{(d\vec{\ell} \times \vec{r})}{4\pi r^3} \tag{1}$$

in which r is the distance from the point to the vortex filament. The magnitude of the induced velocity is given as

$$dV = \frac{\Gamma d\ell r \sin\theta}{4\pi r^3} = \frac{\Gamma d\ell \sin\theta}{4\pi r^2} \tag{2}$$

Referring to figure 5, $r = r_p / \sin\theta$ and $d\ell = r_p(\csc^2\theta)d\theta$. Let $\vec{AB}$ represent the vortex segment with the vorticity vector directed from A to B. Let point C be the point which is the distance r_p directed normally away from segment $\vec{AB}$. Integrating between points A and B gives

$$V = \frac{\Gamma}{4\pi r_p} \int_{\theta_1}^{\theta_2} \sin\theta d\theta = \frac{\Gamma}{4\pi r_p} (\cos\theta_1 - \cos\theta_2) \tag{3}$$

Also from figure 5, $r_p = |\vec{r}_1 \times \vec{r}_2|/r_0$, $\cos\theta_1 = \vec{r}_0 \cdot \vec{r}_1/r_0 r_1$, $\cos\theta_2 = \vec{r}_0 \cdot \vec{r}_2/r_0 r_2$ and the direction of the induced velocity is given by $\vec{r}_1 \times \vec{r}_2/|\vec{r}_1 \times \vec{r}_2|$. Thus,

$$\vec{V} = \frac{\Gamma}{4\pi} \frac{\vec{r}_1 \times \vec{r}_2}{|\vec{r}_1 \times \vec{r}_2|^2} [\vec{r}_0 \cdot (\frac{\vec{r}_1}{r_1} - \frac{\vec{r}_2}{r_2})] \tag{4}$$

Figure 6 shows a typical nth horseshoe vortex on the starboard wing ($y > 0$) for example with filaments $\vec{AD}$, $\vec{AB}$, and $\vec{BC}$ and control point p with coordinates (x,y,z). The position vectors $\vec{r}_0$, $\vec{r}_1$, and $\vec{r}_2$ for vortex filament $\vec{AB}$ are

$$\begin{aligned} \vec{r}_0 &= (x_{2n} - x_{1n})\hat{i} + (y_{2n} - y_{1n})\hat{j} + (z_{2n} - z_{1n})\hat{k} \\ \vec{r}_1 &= (x - x_{1n})\hat{i} + (y - y_{1n})\hat{j} + (z - z_{1n})\hat{k} \\ \vec{r}_2 &= (x - x_{2n})\hat{i} + (y - y_{2n})\hat{j} + (z - z_{2n})\hat{k} \end{aligned} \tag{5}$$

Substituting these vectors into equation (4) and performing the vector algebra yields an expression for the induced velocity, $\vec{V}_{AB}$. Similarly to calculate the induced velocity produced by the vortex filament $\vec{DA}$, the three position vectors are

$$\begin{aligned} \vec{r}_0 &= (x_{1n} - x_{3n})\hat{i} \\ \vec{r}_1 &= (x - x_{3n})\hat{i} + (y - y_{1n})\hat{j} + (z - z_{1n})\hat{k} \\ \vec{r}_2 &= (x - x_{1n})\hat{i} + (y - y_{1n})\hat{j} + (z - z_{1n})\hat{k} \end{aligned} \tag{6}$$

Substituting into equation (4) and letting x_{3n} go to infinity, the induced velocity $\vec{V}_{A\infty}$ is found. The induced velocity from the vortex filament which extends from point B to infinity, $\vec{V}_{B\infty}$, is found in the same manner. The induced velocity at the mth control point $p(x_m, y_m, z_m)$ from the nth horseshoe vortex is then

$$\vec{V}_{m,n} = \vec{V}_{AB} + \vec{V}_{A\infty} + \vec{V}_{B\infty} = \vec{C}_{m,n}\Gamma_n \tag{7}$$

where C is a matrix of influence coefficients representing the induced velocities at the control points.

The total induced velocity at the mth control point is the vector sum of the induced velocities from all of the horseshoe vortices on both the starboard ($y > 0$) and port ($y < 0$) wings. The induced velocity from the nth vortex on the port wing is found in exactly the manner as for the starboard wing with the vortex coordinates interchanged (i.e. x_{1n} and x_{2n} are interchanged, etc.). Flow disturbances created by the fuselage are ignored. For a total of 2N panels, N on both the starboard and port wings, the velocities induced by the horseshoe vortices on the mth control point is

$$\vec{V}_{m,n} = \sum_{n=1}^{2N} \vec{C}_{m,n}\Gamma_n \tag{8}$$

Once the vortex strengths are known, the induced velocity at the control points and hence the forces acting on the wing may be calculated. The vortex strengths are found by applying the flow tangency boundary condition on the mean camber surface of the wing. This boundary condition is

$$\vec{V} \cdot \hat{n} = 0 \tag{9}$$

where $\vec{V}$ represents the freestream velocity, U_∞, plus the induced velocity and $\hat{n}$ is the unit normal to the mean camber surface. For an angle of attack α, the freestream velocity is

$$\vec{U}_\infty = U_\infty \cos\alpha\hat{i} + U_\infty \sin\alpha\hat{k} \tag{10}$$

The induced velocity is written as

$$\vec{V}_{ind} = V_x\hat{i} + V_y\hat{j} + V_z\hat{k} \tag{11}$$

Let the mean camber surface be represented by the function

$$z = F(x,y) \tag{12}$$

or

$$f(x,y,z) = z - F(x,y) = 0 \tag{13}$$

Therefore,

$$\hat{n} = \nabla f = \hat{k} - \frac{\partial F}{\partial x}\hat{i} - \frac{\partial F}{\partial y}\hat{j} \tag{14}$$

The boundary condition is thus

$$\vec{V}\cdot\hat{n} = 0 = U_\infty \sin\alpha - U_\infty \cos\alpha \frac{\partial F}{\partial x} + V_z - V_x \frac{\partial F}{\partial x} - V_y \frac{\partial F}{\partial y} \tag{15}$$

Let ϕ be the slope of the mean camber surface in the x-z plane and ψ be the slope in the y-z plane. Equation (15) can be rewritten as

$$U_\infty \sin\alpha - U_\infty \cos\alpha \tan\phi + V_z - V_x \tan\phi - V_y \tan\psi = 0 \tag{16}$$

or by rearranging, the boundary condition becomes

$$V_z \cos\phi \cos\psi - V_x \sin\phi \cos\psi - V_y \cos\phi \sin\psi = -U_\infty \sin(\alpha - \phi)\cos\psi \tag{17}$$

This equation combined with equation (8) yields a linear system of equations in the form

$$C\vec{\Gamma} = \vec{V} \tag{18}$$

where $\vec{V}$ is a vector representing the normal component of the freestream velocity at each control point. The system of equations can now be solved for the unknown vortex strengths, Γ_n .

2.4 Lift and Drag

The lift and induced drag forces acting on the wing are determined from the vortex strengths using the Kutta-Joukowski theorem. The force per unit width on the ith panel is

$$\vec{F}_i = \rho \vec{V}_i \times \vec{\Gamma}_i \tag{19}$$

where $\vec{\Gamma}_i$ is the vorticity vector on the ith panel. The velocity is written as

$$\vec{V}_i = (U_\infty \cos\alpha + u_i)\hat{i} + v_i\hat{j} + (U_\infty \sin\alpha + w_i)\hat{k} \tag{20}$$

in which u_i, v_i, and w_i are the components of the induced velocity on panel i. The lift and induced drag on the panel which act perpendicular and parallel to the onset flow respectively are

$$L_i = (F_{zi} \cos\alpha - F_{xi} \sin\alpha)\Delta y_i \tag{21}$$

$$D_i = (F_{zi} \sin\alpha + F_{xi} \cos\alpha)\Delta y_i \tag{22}$$

Using the symmetry of the flow, the lift acting on the wing is

$$L = 2\int_0^{b/2} \rho U_\infty \Gamma(y)dy \tag{23}$$

In terms of the finite element panels, the lift is

$$L = 2\rho U_\infty \sum_{n=1}^{N} \Gamma_n \Delta y_n = 2\sum_{n=1}^{N} L_i \tag{24}$$

After having determined the lift and drag forces on the wing, their corresponding coefficients may then be found. The coefficient of lift is

$$C_L = \frac{L}{qS_w} \tag{25}$$

where q is the dynamic pressure and S_w is the wing area. The section lift coefficient defined to be the lift coefficient for a chordwise strip of finite element panels is similarly given as

$$C_\ell = \frac{L_s}{qS_s} \tag{26}$$

where L_s is the sum of the individual panel lift forces of the chordwise strip and S_s is the strip area. The section lift coefficient is used in determining the viscous drag of the wing.

2.5 Viscous Drag

The viscous drag of the wing is determined using the section lift coefficients and the drag polar shown in figure 2. The drag coefficient is assumed to be constant on a wing section. Hence a viscous drag for each section may be found. The total viscous drag is the sum of the section viscous drag forces.

The viscous drag from the fuselage and tail is assumed to be constant. The drag coefficient for the entire aircraft has been obtained for a given reference aircraft (see table 1). The drag coefficient for the fuselage and tail, $C_{Df,t}$, is found by

$$C_{Df,t} = C_{D_{a/c}} - C_{D_{i0}} - C_{D_{v0}} \tag{27}$$

in which $C_{D_{a/c}}$ is the total drag coefficient for the reference aircraft at zero angle of attack, $C_{D_{i0}}$ is the coefficient of induced drag for the wing at zero angle of attack, and $C_{D_{v0}}$ is the viscous drag coefficient for the wing at zero angle of attack.

2.6 Compressibility Correction

The compressibility effects on the wing are determined by using a Gothert transformation. This transformation can be derived beginning with the linearized velocity potential equation,

$$\beta^2 \Phi_{xx} + \Phi_{yy} + \Phi_{zz} = 0 \tag{28}$$

where $\beta \equiv \sqrt{(1 - M_\infty^2)}$. The flow tangency boundary condition is obtained as follows. Let the velocity field $\vec{V}$ be given as

$$\vec{V} = \vec{U}_\infty + \vec{\Phi} = (U_\infty \cos\alpha + \Phi_x)\hat{i} + \Phi_y\hat{j} + (V_\infty \sin\alpha + \Phi_z)\hat{k} \tag{29}$$

and let $F(x,y,z) = 0$ represent the mean camber line of the wing. Thus, the unit normal to the surface is

$$\hat{n} = \nabla F = \frac{\partial F}{\partial x}\hat{i} + \frac{\partial F}{\partial y}\hat{j} + \frac{\partial F}{\partial z}\hat{k} \tag{30}$$

The flow tangency boundary condition is then

$$\vec{V} \cdot \hat{n} = 0 = (U_\infty \cos\alpha + \Phi_x)\frac{\partial F}{\partial x} + \Phi_y \frac{\partial F}{\partial y} + (U_\infty \sin\alpha + \Phi_z)\frac{\partial F}{\partial z} \tag{31}$$

Assuming small angle of attack and that $\Phi_x << U_\infty$ the boundary condition is

$$U_\infty \frac{\partial F}{\partial x} + \Phi_y \frac{\partial F}{\partial y} + (U_\infty \alpha + \Phi_z)\frac{\partial F}{\partial z} = 0 \tag{32}$$

Let the primed quantities represent the incompressible flow over a modified wing with mean camber surface $F'(x', y', z') = 0$. The incompressible coordinates and velocity potential are transformed from the compressible regime as

$$x' = c_1 x\,, \quad y' = c_2 y\,, \quad z' = c_3 z\,, \quad \Phi' = c_4 \Phi \tag{33}$$

The transformed linearized velocity potential equation is

$$\beta^2 \frac{c_1^2}{c_4}\Phi'_{x'x'} + \frac{c_2^2}{c_4}\Phi'_{y'y'} + \frac{c_3^2}{c_4}\Phi_{z'z'} = 0 \tag{34}$$

This defines a relationship between c_1, c_2, and c_3 as

$$\beta c_1 = c_2 = c_3 \tag{35}$$

The transformed boundary condition is

$$c_1 U_\infty \frac{\partial F'}{\partial x'} + \frac{c_2^2}{c_4} \Phi'_{y'} \frac{\partial F'}{\partial y'} + \left(c_3 U_\infty \alpha + \frac{c_3^2}{c_4} \Phi'_{z'}\right) \frac{\partial F'}{\partial z'} = 0 \tag{36}$$

For $c_1 = 1$, $c_2 = c_3 = \beta$ the boundary condition is

$$U_\infty \frac{\partial F'}{\partial x'} + \frac{\beta^2}{c_4} \Phi'_{y'} \frac{\partial F'}{\partial y'} + \left(U_\infty \beta \alpha + \frac{\beta^2}{c_4} \Phi'_{z'}\right) \frac{\partial F'}{\partial z'} = 0 \tag{37}$$

Letting $c_4 = \beta^2$ and $\beta\alpha = \alpha'$, equation (37) becomes

$$U_\infty \frac{\partial F'}{\partial x'} + \Phi'_{y'} \frac{\partial F'}{\partial y'} + \left(U_\infty \alpha' + \Phi'_{z'}\right) \frac{\partial F'}{\partial z'} = 0 \tag{38}$$

By comparison to the compressible flow boundary condition, this is exactly the boundary condition of the incompressible flow on the surface F'. Therefore, to use the vortex-lattice method to determine the forces acting on the wing, the x, y, and z coordinates and the angle of attack, α, are first transformed according to

$$x' = x\,, \quad y' = \beta y\,, \quad z' = \beta z\,, \quad \alpha' = \beta\alpha \tag{39}$$

We may then proceed with the solution as though the problem is an incompressible one.

In order to extend the force calculations from the incompressible to the compressible flow field, the linearized pressure coefficient is used. The linearized pressure coefficient for potential flow is

$$C_p = -\frac{2}{U_\infty}\Phi_x \tag{40}$$

Transforming this gives

$$C_p = -\frac{2}{U_\infty}\frac{c_1}{c_4}\Phi'_{x'} = -\frac{2}{U_\infty}\frac{1}{\beta^2}\Phi'_{x'} \tag{41}$$

or

$$C_p = \frac{C'_p}{\beta^2} \tag{42}$$

Since the lift and drag forces result from the integration of the pressure distribution over the surface of the wing, the incompressible-compressible relation for those coefficients is

$$C_L = \frac{C'_L}{\beta^2}\ ,\ C_D = \frac{C'_D}{\beta^2}\quad . \tag{43}$$

3.0 Aeroelastic Analysis

The coupling between the aerodynamic loads on the wing and the resulting associated structural deformations form the basis for the aeroelastic analysis. In order to simplify this analysis several assumptions must be made. First it is assumed that the effect of the aerodynamic loads may be lumped at n_l specified structural nodes known as the load set. Next it is assumed that only the vertical forces on the wing produce structural deformation and that the response of the aircraft affects the wing only through the root angle of attack. Finally, it is assumed that the effect of the structural deformation upon the aerodynamic response may be modeled by vertical displacements at the load set.

The aerodynamic forces are calculated using the formulation described in section 2.3. The vertical aerodynamic forces located on the vortex lattice panels, F_z, are grouped at the load set by

$$F_a = EF_z = f_1(p, \alpha, \theta) \tag{44}$$

in which F_a is the vector of the vertical forces of length n_l , and E is a transformation matrix. F_a is a function of the design parameters p, angle of attack α, and the

structural vertical displacements θ. The transformation matrix is determined by the equilibrium equations

$$\sum_{i=1}^{n_l} F_{ai} = \sum_{j=1}^{NTP} F_{zj}$$

$$\sum_{i=1}^{n_l} F_{ai} \cdot x_i = \sum_{j=1}^{NTP} F_{zj} \cdot x_j \tag{45}$$

$$\sum_{i=1}^{n_l} F_{ai} \cdot y_i = \sum_{j=1}^{NTP} F_{zj} \cdot y_j$$

where NTP is the number of aerodynamic panels on the wing. Each vertical force F_{zj} is distributed to three nearby and surrounding load set nodes by using the previous equilibrium equations. The three load set nodes form a triangle which encompasses the aerodynamic node j as illustrated in figure 7. This is vital to the physical aspect of the modeling. If the aerodynamic node were to lie outside of the triangular region, there would be a negative or downward contribution of the force from node j onto the load set nodes. For aerodynamic nodes which happen to lie on a boundary of two triangular regions, the one with the load set nodes closest to the aerodynamic point is used.

The angle of attack is obtained from the aircraft vertical equilibrium equation

$$f_2(p, \theta) = \tfrac{1}{2} nW - N^T F_a = 0 \tag{46}$$

in which n is the load factor (1.0 for cruise, 2.5 for maneuver), W is the weight of the aircraft, and N is a summation vector.

The vertical displacements at the load set are calculated by finite element analysis using a modification of the WIDOWAC program (Ref. 10). First the nodal displacement vector U is found by solving

$$K(p)U = TF_a + nF_I(p) \tag{47}$$

where K is the stiffness matrix, T is a Boolean matrix which expands F_a to the full set of structural degrees of freedom, and F_I is the gravitational and inertial load vector. The stresses and strains are then calculated from the displacement vector, U. The vertical displacements, θ, are extracted from U by

$$\theta = T^T U \tag{48}$$

These two equation are combined to give

$$\theta = f_3(p,F_a) \tag{49}$$

3.1 Solution Procedure

Equations (44), (46), and (49) are a set of nonlinear coupled equations for the vertical aerodynamic loads, F_a, the wing root angle of attack, α, and the vertical structural displacements, θ . For the analysis problem, the design variables p are given. Reference (5) presents a modular sensitivity analysis of such coupled interdisciplinary equations. In this modular approach the individual discipline analysis procedures are treated in a "black box" fashion. These procedures do not need to be changed in the integration procedure. A similar approach is employed for

the sensitivity analysis with f_1 representing the aerodynamic black box, and f_3 representing the structural black box. The same approach is employed for the solution of the system via Newton's method.

Given an initial estimate for the solution F_a^0, α^0 , θ^0 to the coupled nonlinear system of equations, Newton's method is used to improve that estimate. The iterative process can be written as

$$J\Delta Y = \Delta f \tag{50}$$

where

$$\Delta Y = \begin{Bmatrix} \Delta F_a \\ \Delta\alpha \\ \Delta\theta \end{Bmatrix} \tag{51}$$

and

$$\Delta f = \begin{Bmatrix} f_1(p, \alpha^0, \theta^0) - F_a^0 \\ f_2(p, F_a^0) \\ f_3(p, F_a^0) - \theta^0 \end{Bmatrix} \tag{52}$$

and the Jacobian J is

$$J = \begin{bmatrix} I & \frac{-\partial f_1}{\partial\alpha} & \frac{-\partial f_1}{\partial\theta} \\ \frac{-\partial f_2}{\partial F_a} & 0 & 0 \\ \frac{-\partial f_3}{\partial F_a} & 0 & I \end{bmatrix} = \begin{bmatrix} I & -qR & -qA \\ N^T & 0 & 0 \\ -S & 0 & I \end{bmatrix} \tag{53}$$

In the Jacobian, q is the dynamic pressure, R is the incremental aerodynamic force vector with components r_i, A is the aerodynamic influence coefficient matrix with

components a_{ij} , and S is the flexibility matrix with components s_{ij}. The incremental aerodynamic force vector is defined such that qr_i represents the change in vertical force at load set node i, F_{ai}, due to a unit change in angle of attack, α. The aerodynamic influence coefficient matrix is defined such that qa_{ij} is the change in F_{ai} due to a unit vertical displacement at load set node j, θ_j. Similarly the flexibility matrix element, s_{ij} , is the change in θ_j due to a unit change in F_{aj}.

Partial solution of equation (50) gives the following three equations for the increments $\Delta\theta$, $\Delta\alpha$, ΔF_a:

$$(I - qSA^*)\Delta\theta = SB\Delta f_1 + \frac{SR}{N^TR}\Delta f_2 + \Delta f_3 \tag{54}$$

$$\Delta\alpha = \frac{\Delta f_2 - N^T\Delta f_1 - qN^TA\Delta\theta}{qN^TR} \tag{55}$$

$$\Delta F_a = \Delta f_1 + qR\Delta\alpha + qA\Delta\theta \tag{56}$$

where B is defined as

$$B \equiv I - \frac{RN^T}{N^TR} \tag{57}$$

and $A^* \equiv BA$.

For the transport design, the initial estimate is a rigid wing approximation $F_a^0 = F_{ar}$, $\alpha^0 = \alpha_r$, and $\theta^0 = 0$, where

$$F_{ar} = f_1(p,0,0) + q\alpha_r R \tag{58}$$

$$\alpha_r = \frac{\frac{1}{2}nW - f_1(p,0,0)}{qN^TR} \tag{59}$$

F_{ar} is the rigid force approximated by a linear extension in α from the base condition of zero angle of attack and no structural deformation. α_r is the rigid angle of attack. A single Newton's iteration from this point is executed to approximate the flexible wing response.

3.2 *Aeroelastic Divergence*

The aeroelastic divergence instability is calculated at a fixed angle of attack because it is assumed that the pilot does not react fast enough to change the angle of attack as the wing diverges. This is characterized by

$$\begin{bmatrix} I & -qA \\ -S & I \end{bmatrix} \begin{Bmatrix} \Delta F_a \\ \Delta \theta \end{Bmatrix} = 0 \tag{60}$$

which is a homogeneous solution to equation (50). This is recognized as an eigenvalue problem for q. The lowest eigenvalue is the divergence dynamic pressure, q_D. Equation (60) can be reduced to a standard linear eigenproblem by substituting the second equation into the first to yield

$$(AS - \frac{1}{q} I) \Delta F_a = 0 \tag{61}$$

The solution to equation (60) is denoted as $\{F_{aD}, \theta_D\}^T$ and is given as

$$\begin{bmatrix} I & -q_D A \\ -S & I \end{bmatrix} \begin{Bmatrix} F_{aD} \\ \theta_D \end{Bmatrix} = 0 \tag{62}$$

This eigenvalue problem also has a left eigenvector $\{F_{aL}^T, \theta_L^T\}$ and the solution is given as

$$\left\{ F_{aL}^T, \theta_L^T \right\} \begin{bmatrix} I & -q_D A \\ -S & I \end{bmatrix} = 0 \tag{63}$$

3.3 *Aeroelastic Sensitivities*

It is common practice to follow the procedure described in section 3.1 and use a single Newton's iteration in the flexible wing analysis. Then for the integrated design problem in which derivatives with respect to a design parameter p are required, equations (54), (55), and (56) are differentiated with respect to p (e.g. Ref. 4). This approach requires the derivatives of the A and S matrices which is computationally expensive. Instead, the method of reference 5 is followed and equations (44), (46), and (49) are differentiated with respect to p to give

$$JY' = f' \tag{64}$$

where prime denotes differentiation with respect to p. Thus, Y' is

$$Y' = \begin{Bmatrix} F'_a \\ \alpha' \\ \theta' \end{Bmatrix} \tag{65}$$

and f' is

$$f' = \begin{Bmatrix} f'_1 \\ f'_2 \\ f'_3 \end{Bmatrix} \tag{66}$$

The Jacobian matrix J in equation (64) is the same matrix utilized in the analysis in equation (50). Equation (64) can be partially solved to yield

$$(I - qSA^*)\theta' = SBf'_1 + \frac{SR}{N^TR} f'_2 + f'_3 \tag{67}$$

$$\alpha' = \frac{f'_2 - N^Tf'_1 - qN^TA\theta'}{qN^TR} \tag{68}$$

$$F'_a = f'_1 + qR\alpha' + qA\theta' \tag{69}$$

This method does not require any derivatives of the A and S matrices, but only partial derivatives of f_1, f_2, and f_3 . For example, f'_1 denotes the derivative of F_a with respect to a design parameter when α and θ are fixed.

By contrast, the more traditional approach (e.g. Ref. 4) to the derivative calculation is obtained by differentiating the aeroelastic analysis equations, such as equations (54) to (56) with respect to p. For example, consider the derivative of equation (54) with respect to p

$$(I - qSA^*)\Delta\theta' = qS'A^*\Delta\theta + qSA'B\Delta\theta + qSAB\Delta\theta + S'B\Delta f_1$$

$$+ SB'\Delta f_1 + SB\Delta f_1 + \frac{S'R}{N^TR}\Delta f_2 + S(\frac{R}{N^TR})'\Delta f_2 \tag{70}$$

$$+ \frac{SR}{N^TR}\Delta f'_2 + \Delta f'_3$$

This complicated expression can be shown to be equivalent to equation (67). Thus, the traditional approach requires the expensive calculation of the derivatives of both the aerodynamic influence coefficient matrix A' and the flexibility matrix S' .

To find the derivative of the divergence dynamic pressure q_D with respect to a design parameter p, equation (60) is differentiated giving

$$\begin{bmatrix} I & (-q_D A)' \\ -S' & I \end{bmatrix} \begin{Bmatrix} F_{aD} \\ \theta_D \end{Bmatrix} + \begin{bmatrix} I & -q_D A \\ -S & I \end{bmatrix} \begin{Bmatrix} F'_{aD} \\ \theta'_D \end{Bmatrix} = 0 \tag{71}$$

Premultiplying this equation by the left eigenvector $\{F_{aL}^T , \theta_L^T\}$ results in the second term in the equation dropping out leaving only

$$\{ F_{aL}^T , \theta_L^T \} \begin{bmatrix} I & -(q_D A)' \\ -S' & I \end{bmatrix} \begin{Bmatrix} F_{aD} \\ \theta \end{Bmatrix} = 0 \tag{72}$$

or solving for q'_D

$$q'_D = - \frac{q_D F_{aL}^T A' \theta_D + \theta_L^T S' F_{aD}}{F_{aL}^T A \theta_D} \tag{73}$$

Equation (73) contains derivatives of the aerodynamic matrix, A, and the flexibility matrix, S, which have so far been avoided. However, these terms may be simplified. Using the definition of A,

$$A' \theta_D = \frac{\partial}{\partial p} \left(\frac{\partial f_1}{\partial \theta} \right) \theta_D \tag{74}$$

To illustrate how $A'\theta_D$ can be calculated without calculating A' consider a generic case. Let f be a function of a vector X and let D be another vector. Let X_0 be a particular choice for X, then

$$\frac{\partial f}{\partial x} (X_0) D = \lim_{\varepsilon \to 0} \frac{[f(X_0 + \varepsilon D) - f(X_0)]}{\varepsilon}$$

$$= \frac{d}{d\varepsilon} f(X_0 + \varepsilon D) \tag{75}$$

This is the definition of a directional derivative and provides for the calculation of the product $\frac{\partial f}{\partial x}(X_0)$ times D without having to calculate the individual components of $\frac{\partial f}{\partial x}$. To calculate $A'\theta_D$, the derivative of f_1 to a perturbation in θ in the form of θ_D is first obtained. Then the derivative of this response with respect to p is found assuming that θ_D is fixed. The term $S'F_{aD}$ in equation (73) is treated in a similar fashion.

4.0 Numerical Optimization Procedure

The basic optimization algorithm is a sequence of unconstrained minimizations using Newton's method with approximate derivatives for function minimizations. This is accomplished by transforming the constrained minimization problem into an unconstrained minimization through the use of an extended interior penalty function. The optimizer used for the wing design is NEWSUMT-A (Ref. 11).

The general problem formulation is :

Minimize $f(x_1, x_2, ..., x_{NDV})$

subject to $g_q(x_1, x_2, ..., x_{NDV}) \geq 0, \quad q = 1, 2, ..., n_{ineq}$

and $h_q(x_1, x_2, ..., x_{NDV}) = 0, \quad q = 1, 2, ..., n_{eq}$

where f is the objective function as a function of the NDV design variables $[x_1, x_2, ..., x_{NDV}]$, g_q and h_q are the inequality and equality constraints respectively. A move limit strategy is used giving rise to upper and lower bounds on the design variables, i.e. $x_i^l \leq x_i \leq x_i^u$, i = 1,2,...,NDV. An initial design point in the design space is specified by giving numerical values for the initial design variable vector $\vec{X}_0$. NEWSUMT-A then modifies the design variables generating a sequence of vectors such that either the objective function decreases or the degree of constraint

satisfaction is improved. The sequence converges to $\vec{X}_f$ where the degree of constraint violation is small and $f(\vec{X}_f)$ is at least a local minimum.

4.1 Forward-Swept Wing Design Optimization

The design problem for the forward-swept wing formulation is :

$$\begin{aligned} &\text{Minimize} && W_G(p) \\ &\text{such that} && g_s(p) \geq 0 \\ & && V_s(p) \geq V_r \\ &\text{and} && R_g(p,D) \geq R_{ref} \end{aligned}$$

where W_G is the gross weight of the aircraft and g_s are constraints on structural stresses, strains, and aeroelastic stability. V_s and V_r are the calculated volume of the wing and the required fuel volume respectively. R_g is the calculated range (see Appendix) and is required to be greater than or equal to the range of the reference aircraft, R_{ref}.

The gross weight of the aircraft is

$$W_G = W_S + W_{UF} + W_P \tag{76}$$

in which W_S is the aircraft standard empty weight, W_{UF} is the usable fuel weight, and W_P is a payload weight. W_S is calculated by

$$W_S = W_{RS} - (W_{RW} - W_W)\cdot\eta \tag{77}$$

W_{RS} is the reference aircraft standard empty weight, W_{RW} is the reference aircraft wing weight, and W_w is the calculated wing weight. The structural weight savings factor, η , is introduced to account for additional weight savings such as in the tail and engines due to reduced wing weight. For this design η is chosen to be 2. Hence, for saving one newton in the wing, an additional newton is saved in other structural components.

The aerodynamic design variables consist of the six planform variables shown in figure 1 and the twist distributions for both the inboard and outboard wing regions. Two performance design variables are the cruise dynamic pressure and the usable fuel weight. During the design optimization the cruise velocity is held constant forcing changes in the dynamic pressure to correspond to changes in freestream density. In this regard the optimization indirectly produces an optimum cruise altitude.

The structural design variables are the skin thicknesses, spar cap areas, and ply orientation. The structure is designed to withstand a 2.5g pull-up maneuver with a 1.5 factor of safety. Maximum strain constraints are imposed on each composite lamina and a maximum stress constraint is imposed on the spar caps. The aeroelastic constraint is that the divergence speed is at least 1.2 times the maneuver speed.

There are two performance constraints: (1) that the range of the aircraft is at least that of the reference aircraft, and (2) that the wing volume be enough to carry the necessary fuel during the flight. There are a total of 39 design variables and 307 constraints. Tables 2 and 3 present the complete lists of the design variables and constraints respectively.

Previous work has shown that for the integrated design problem a sequential approximate optimization algorithm is superior to an optimization algorithm which is linked directly to the analysis code (Ref. 12). In this approach, the objective function and constraints are evaluated by approximations based on nominal values and derivatives at an initial point. The move limits keep the design bounded such that the approximations remain valid. In addition, since the range calculation is relatively expensive, it is calculated based on a linear approximation of the drag. The approximate optimization problem can be written as :

$$\text{Minimize} \quad W_c(p)$$

$$\text{such that} \quad g_s^0 + \sum_{i=1}^{NDV} \frac{\partial g_s}{\partial p_i}(p_i - p_i^0) \geq 0$$

$$V_s(p) \geq V_r$$

$$R_g(p,D) \geq R_{ref}$$

$$\text{with} \qquad D = D^0 + \sum_{i=1}^{NDV} \frac{\partial D}{\partial p_i}(p_i - p_i^0)$$

Figure 8 shows the linear drag approximation versus the exact drag for one approximate optimization cycle. For clarity, the drag is written as

$$D = f_4(p, \alpha, \theta) \tag{78}$$

Differentiating this equation yields the drag sensitivities used for the linear approximation of the drag force,

$$\frac{\partial D}{\partial p} = \frac{\partial f_4}{\partial p} + \frac{\partial f_4}{\partial \alpha}\frac{\partial \alpha}{\partial p} + \frac{\partial f_4}{\partial \theta}\frac{\partial \theta}{\partial p} \tag{79}$$

4.2 Design Program

Figure 9 illustrates the overall wing design process. The process begins with an initialization module which defines the design variables and parameters. Next the geometry of the wing and the load set nodes are defined. The aerodynamic and structural flexibility analyses are then independently performed yielding the A and S matrices, and the R vector. Next the aeroelastic/sensitivity analyses at both cruise and maneuver flight conditions is performed giving the drag sensitivities at cruise and the structural stress, strain and divergence sensitivities at maneuver. Finally, the optimization is run using the design analyses and sensitivities previously calculated. If the gross weight of the aircraft has converged the optimization is complete. If not, the process is repeated until convergence.

The flow chart for the aeroelastic/sensitivity analysis for cruise is shown in figure 10. The aeroelastic analysis yields F_a, α , and θ which are used to find f_1, f_2 , and f_3. Derivatives of the f_i with respect to the design variables are found by finite differencing. The modular sensitivity analysis is performed giving F'_a, α', and θ'. The drag sensitivities are then found using equation (79).

Figure 11 shows the flow chart for the aeroelastic/sensitivity analysis for the maneuver flight condition. The aeroelastic analysis is performed and the f'_i are found in the same manner as the cruise analysis. The right and left eigenvectors and the divergence dynamic pressure are then found. These are used to obtain $S'F_{aD}$ and $A'\theta_D$. The modular sensitivity analysis then gives F'_a, α', and θ' . These quantities are then used to find the structural stress and strain sensitivities used to guide the optimization procedure.

4.3 Discussion of Results

The initial and final designs of the transport wing are given in table 4. The initial design is obtained by replacing the backward-swept of the reference aircraft with a forward-swept wing. The final design was reached in 7 optimization cycles. The weight convergence is plotted in figure 12. The initial gross weight of the aircraft of 4.391×10^5 N is reduced to 4.150×10^5 N, a savings of 5.5 percent. However, this percentage misrepresents the relative weight savings in the wing since the wing weight is only a small percentage of the total weight. The reduction in the gross weight of 2.410×10^4 N is accounted for by the difference in structural weight multiplied by the structural weight savings factor, η, plus the weight savings in usable fuel. The initial structural wing weight of 2.779×10^4 N is reduced to 1.728×10^4 N for a savings for 37.8 percent and the usable fuel weight is reduced from 2.190×10^4 N to 1.876×10^4 N. The range of the initial design exceeds that of the reference aircraft by 17 percent while the range of the final design has been brought to within 1 percent of the reference range. Again, the range constraint imposed is that the final design should have the same range as the reference aircraft. The difference in range between the initial design and the reference aircraft is due to the fact that the transport is designed to fly at Mach 0.48 versus the design Mach number of 0.78 of the reference aircraft. The 1 percent residual in the range at the final design is evidence that the design is not yet fully converged and is probably due to the poor initial design. Also, throughout the design optimization, restrictive move limits were required, particularly in the later optimization cycles, in order to keep the drag approximation accurate. This precipitated only slight reductions in the gross weight at substantial computational expense. The 6 geometric planform design variables are

all decreased from the initial design for a reduction in wing area of 23.8 percent. These results should be viewed as preliminary to a more refined design to be presented in a future paper.

5.0 Concluding Remarks

This thesis concentrates on presenting an analysis method for use in an integrated aerodynamic-structural wing design. The utilization of composite materials requires the use of such integrated design techniques. These techniques allow designers an avenue for effectively utilizing the natural responses of the system to improve design performance and effectiveness or guard against unwanted behavior.

Previous research has demonstrated the advantages of the integrated design technique via production of designs superior to those obtained using the traditional sequential method. Associated with refinement of the analysis methods is increased computational expense. Since most systems are of appreciable size, reduction of these expenses is vital to the practicality of the design method whether it be an integrated or sequential technique. The use of perturbation methods and an approximate optimization technique proved to be effective cost reduction techniques for the sailplane design. However, the additional complexity associated with the analysis employed for the forward-swept wing transport required further cost reduction.

This research presented the application of a modular sensitivity approach and the results of this method for the design optimization of a subsonic, forward-swept wing transport. By treating the system in a "black box" fashion, this method provides a certain degree of decoupling between the disciplines involved in the design process. That is to say that each discipline can be viewed as an independent subsystem of the integrated design problem. A direct result of this decoupling is an efficient method for calculating the derivatives used for obtaining the solution of the system via Newton's method and for guiding an optimization.

It is to be understood that the emphasis in this work lies upon presenting the method as an efficient computational technique and that the design results are merely an indication of the soundness of the method and are not necessarily a practical design. Continuing research will present the use of this technique with a more detailed and lifelike design problem. This will include optimized airfoil shape, transonic flight, and dynamic aeroelastic constraints will be considered. The airfoil shape optimization, in addition to increasing the complexity of the optimization procedure, requires a three-dimensional boundary layer solution for obtaining the drag force since experimentally obtained drag polars will be unavailable. The analysis for transonic flight requires non-linear computations over the entire flow field. This analysis alone will require a minimum estimated order of magnitude increase in CPU time over the vortex-lattice method. Also, the addition of controls to the existing integrated design optimization will be considered resulting in a coupling of three disciplines. These additions warrant the investigation of more efficient algorithms to further reduce the computational burden.

Appendix A. Range Calculation

Neglecting the small effect of changes in elastic deformation due to change in the weight over one optimization cycle the drag may be written as

$$D = qS_wC_D(C_L) \tag{1}$$

where C_D is the drag coefficient of the wing. The coefficient of lift is

$$C_L = \frac{L}{qS_w} = \frac{W}{qS_w} \tag{2}$$

where W is the design weight of the aircraft. To find the optimum dynamic pressure, q_m, and hence optimum altitude, equation (1) is differentiated with respect to q and set equal to zero yielding

$$\frac{dD}{dq} = S_wC_D + q_mS_w\frac{dC_D}{dC_L}\frac{dC_L}{dq} = 0 \tag{3}$$

Using equation (2),

$$\frac{dC_L}{dq} = -\frac{W}{S_w q^2} \tag{4}$$

Substituting this into equation (3) and solving for q_m gives

$$q_m = \frac{W}{S_w C_D}\frac{dC_D}{dC_L} \tag{5}$$

Substituting q_m into equation (1) yields the drag at the optimum altitude and the design weight corresponding to the half-fuel condition, W_0, to be

$$D_m = W_0 \frac{dC_D}{dC_L} = \kappa W_0 \tag{6}$$

The range is calculated based on this assumption that the drag is proportional to the weight of the aircraft. The rate of change of the aircraft weight due to fuel burning is

$$\frac{dW}{dt} = -c'T = -c'D_m = -c'\kappa W \tag{7}$$

in which c′ is the thrust specific fuel consumption and T is the thrust. Integrating equation (7) between the initial time t_i and final time t_f gives

$$\ln\left(\frac{W_f}{W_i}\right) = -c'\kappa(t_f - t_i) \tag{8}$$

Since it is assumed that the aircraft is flying at constant cruise speed V_c , the cruise range is

$$R_g = V_c(t_f - t_i) = \frac{V_c}{c'\kappa}\ln\left(\frac{W_i}{W_f}\right) = \frac{V_c}{c'}\frac{W_0}{D_m}\ln\left(\frac{W_i}{W_f}\right) \tag{9}$$

Hence the calculated range for the wing design is proportional to the design weight and drag of the aircraft.

References

1. Haftka, R. T., "Structural Optimization with Aeroelastic Constraints A Survey of US Applications",International Journal of Vehicle Design, Vol. 7, 1986, pp. 381-392.

2. Shirk, M. H., Hertz, T. J. and Weisshar, T. A., "A survey of Aeroelastic Tailoring - Theory, Practice, and Promise", Journal of Aircraft, Vol. 23, No. 1, Jan 1986, pp. 6-18.

3. Grossman, B., Strauch, G. J., Eppard W. M., Gurdal, Z. and Haftka, R. T., "Combined Aerodynamic-Structural Design of a Sailplane Wing", "Journal of Aircraft", Vol. 25, No. 9, 1988, pp. 855-860.

4. Haftka, R. T., Grossman, B., Eppard, W. M., Kao, P. J. and Polen, D. M., "Efficient Optimization of Integrated Aerodynamic-Structural Design", Proceedings of 2nd Intl. Conf. on Inverse Design Concepts and Optimization in Engineering Sciences, Oct. 1987, pp. 369-386 (also "International Journal of Numerical Methods in Engineering", Vol. 28, 1989, pp. 593-607).

5. Sobieszczanski-Sobieski, J., "On the Sensitivity of Complex, Internally Coupled Systems", AIAA Paper No. 88-2378, Presented at the AIAA/ASME/ASCE/AHE 29th Structures, Structural Dynamics and Materials Conference, Apr. 1988.

6. Sobieszczanski-Sobieski, J. and Haftka, R. T., "Interdisciplinary and Multilevel Optimum Design", Proceedings of the NATO Advanced Study Institute on Computer Aided Optimal Design : Structural and Mechanical Systems, Edited by C. A. Mota Soares, Springer-Verlag, 1987.

7. Viken, J. K., et. al., "Wind Tunnel Results for a High-Speed, Natural Laminar-Flow Airfoil Designed for General Aviation Aircraft", NASA TM-87602, Nov. 1987.

8. Kao, P. J., "Efficient Methods for Integrated Structural-Aerodynamic Wing Optimum Design", PhD Dissertation, Virginia Polytechnic Institute and State University, March 1989.

9. Bertin, J. J. and Smith, M. L., "Aerodynamics for Engineers", Prentice Hall Inc., 1979.

10. Haftka, R. T. and Starnes, J. H. Jr., "WIDOWAC : Wing Design Optimization with Aeroelastic Constraints - Program Manual", NASA TM X-3071, 1974.

11. Grandhi, R. V., Thareja, R. and Haftka, R. T., "NEWSUMT - A : A General Purpose Program for Constrained Optimization Using Constraint Approximations", ASME J. Mech., Trans. & Automation in Design, Vol. 107, 1985, pp. 94-107.

12. Schmit, L. A. and Farshi, B., "Some Approximation Concepts for Structural Synthesis", AIAA J., 12, 1974, pp. 692-699.

13. Eppard, W. M., "Integrated Aerodynamic-Structural Design Optimization", MS Thesis, Virginia Polytechnic Institute and State University, June 1987.

14. Haftka, R. T., Grossman, B., Kao, P. J., Polen, D. M. and Sobieszczanski-Sobieski, J, "Integrated Aerodynamic-Structural Design of a Forward-Swept Transport Wing", Proc. of Second NASA/Air Force Symposium on Recent Experiences in Multidisciplinary Analysis and Optimization, Sept. 28-30, 1988.

15. Haftka, R. T., Grossman, B., Kao, P. J., Polen, D. M. and Sobieszczanski-Sobieski, J, "Integrated Structural-Aerodynamic Design Optimization", Proc. of 10th Congress of the Intl. Council of Aero. Sci., ICAS-88-1.10R, Aug 1988, pp. 1820-1825.

16. Rais-Rohani, M., private communication.

Table 1. Reference Aircraft Design Specifications

Weight, (N):	
W_G	4.494×10^5
W_{RS}	2.852×10^5
W_{UF}	2.738×10^4
W_P	1.368×10^5
W_{RW}	3.020×10^4
Wing:	
Aspect Ratio	14
Area, m^2	83.98
Span, m	34.29
Thickness, %	12
Sweep at c/4, deg.	15
Taper Ratio	.25
Horizontal Tail Area, m^2	11.71
Vertical Tail Area, m^2	17.74
Average Cruise:	
Mach No.	.78
Lift Coeff.	.672
Drag Coeff.	.014
L/D (Lift to Drag Ratio)	20.7
c′ (Specific Fuel Consumption)	.430
Range, m:	2.34×10^6

Table 2. Forward-Swept Wing Design Variables

8 Geometric Design Variables	1. Chord length at the root
	2. Chord length at the break
	3. Chord length at the tip
	4. Distance to the break
	5. Distance from break to tip
	6. Sweep angle at the break
	7. Twist angle at the break
	8. Twist angle at the tip
2 Performance Design Variables	9. Dynamic pressure at cruise
	10. Usable fuel weight
29 Structural Design Variables	11-34. Panel thicknesses
	35-38. Spar cap areas
	39. Ply orientation

Table 3. Forward-Swept Wing Design Constraints

305 Structural Constraints	1-228. Maximum strain in composite skin
	229-304. Maximum spar cap stresses
	305. Divergence dynamic pressure
2 Performance Constraints	306. Range
	307. Enough volume for fuel

Table 4. Initial and Final Designs for Forward-Swept Transport Wing

	Initial Design	Final Design
Gross Weight (N)	4.391×10^5	4.150×10^5
Wing Weight (N)	2.779×10^4	1.728×10^4
Usable Fuel Weight (N)	2.190×10^4	1.876×10^4
Range Margin from Reference	17%	1%
Chord Lengths (m)		
Root	6.916	5.912
Break	3.765	3.218
Tip	1.725	1.234
Distance from Root to Break (m)	5.754	4.918
Distance from Break to Tip (m)	12.250	10.443
Sweep Angle(deg.)	26.1	18.8

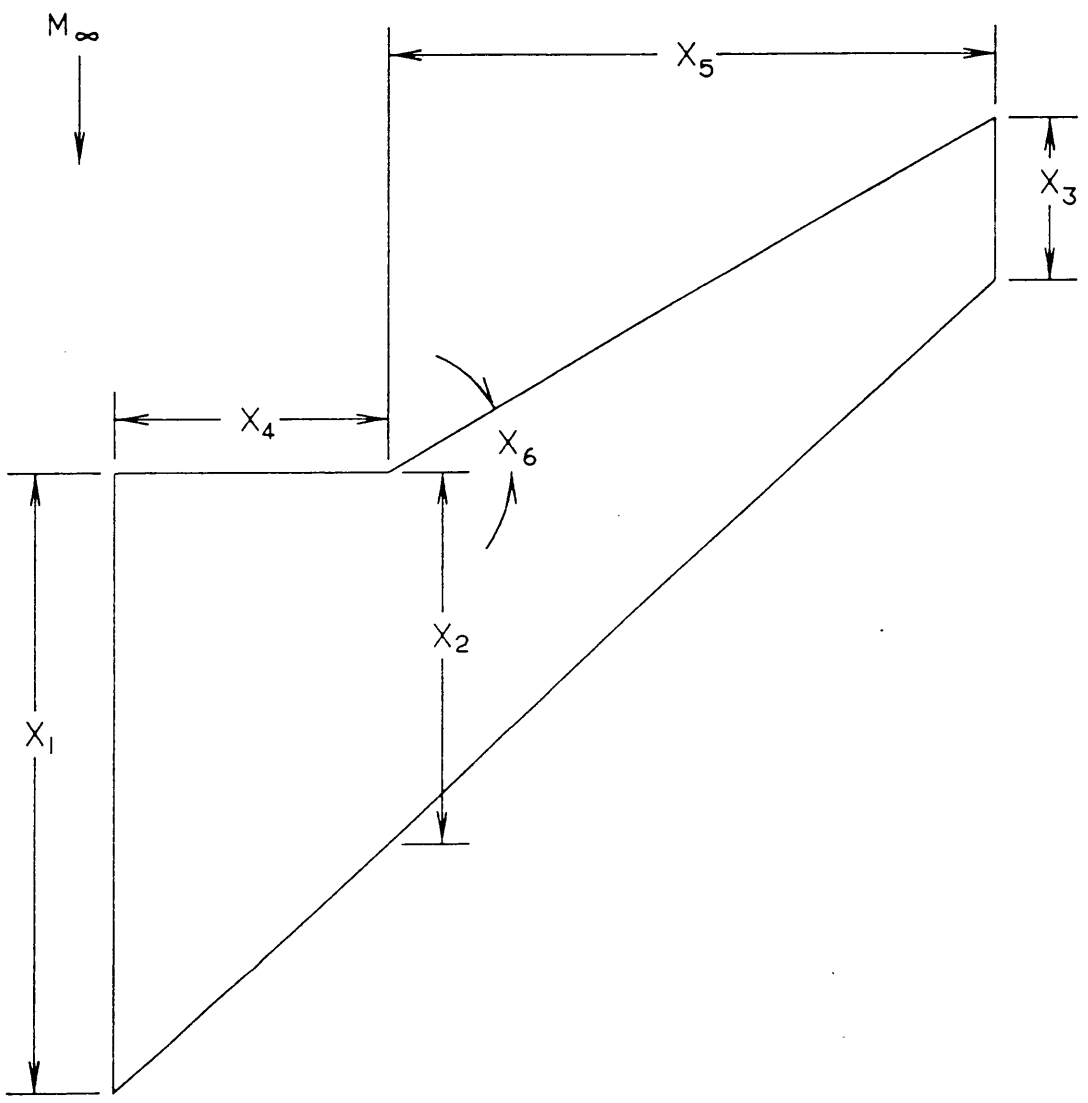

Figure 1. Planform Design Variables

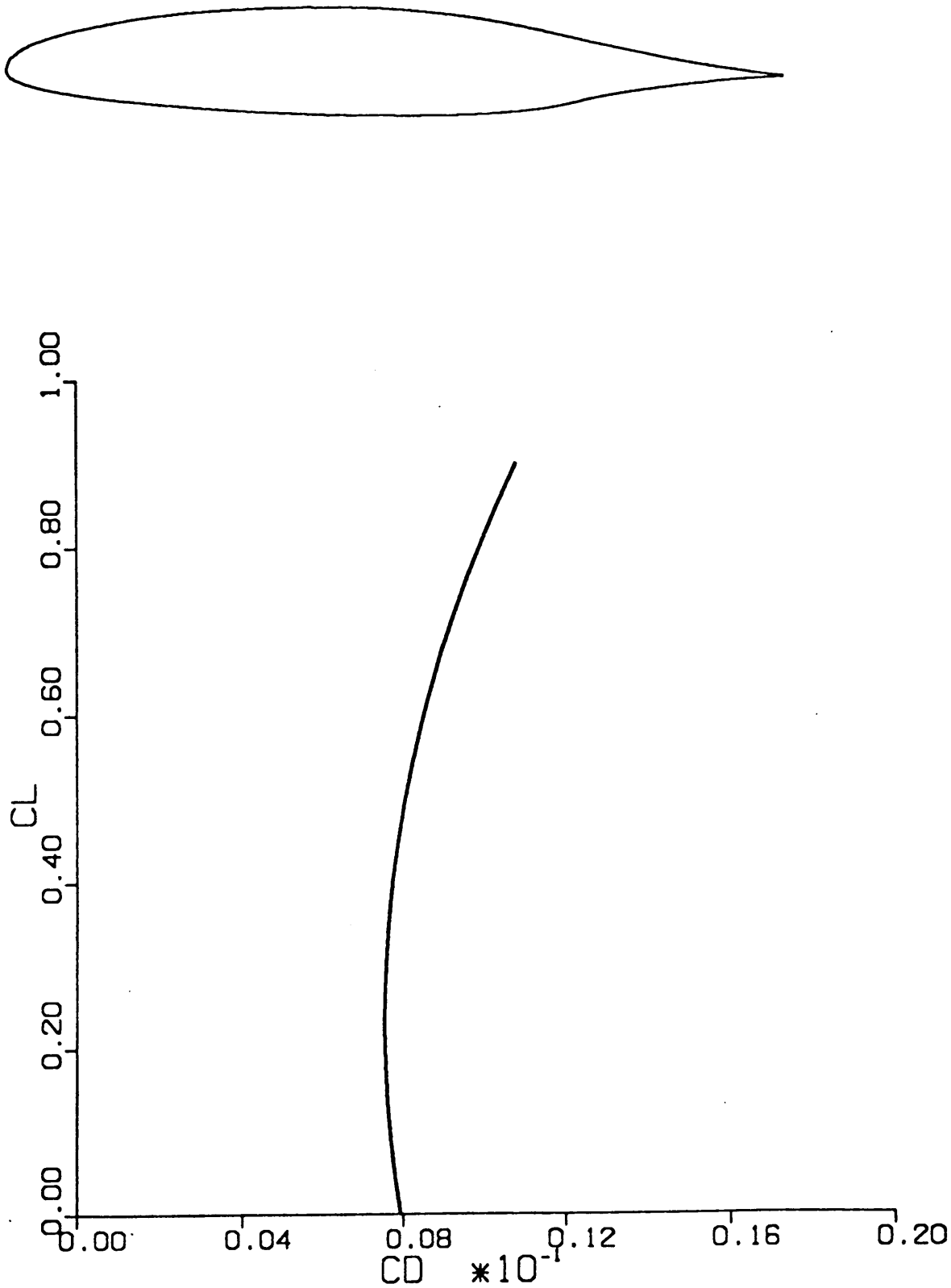

Figure 2. HSNLF(1)-0213 Airfoil and Drag Polar

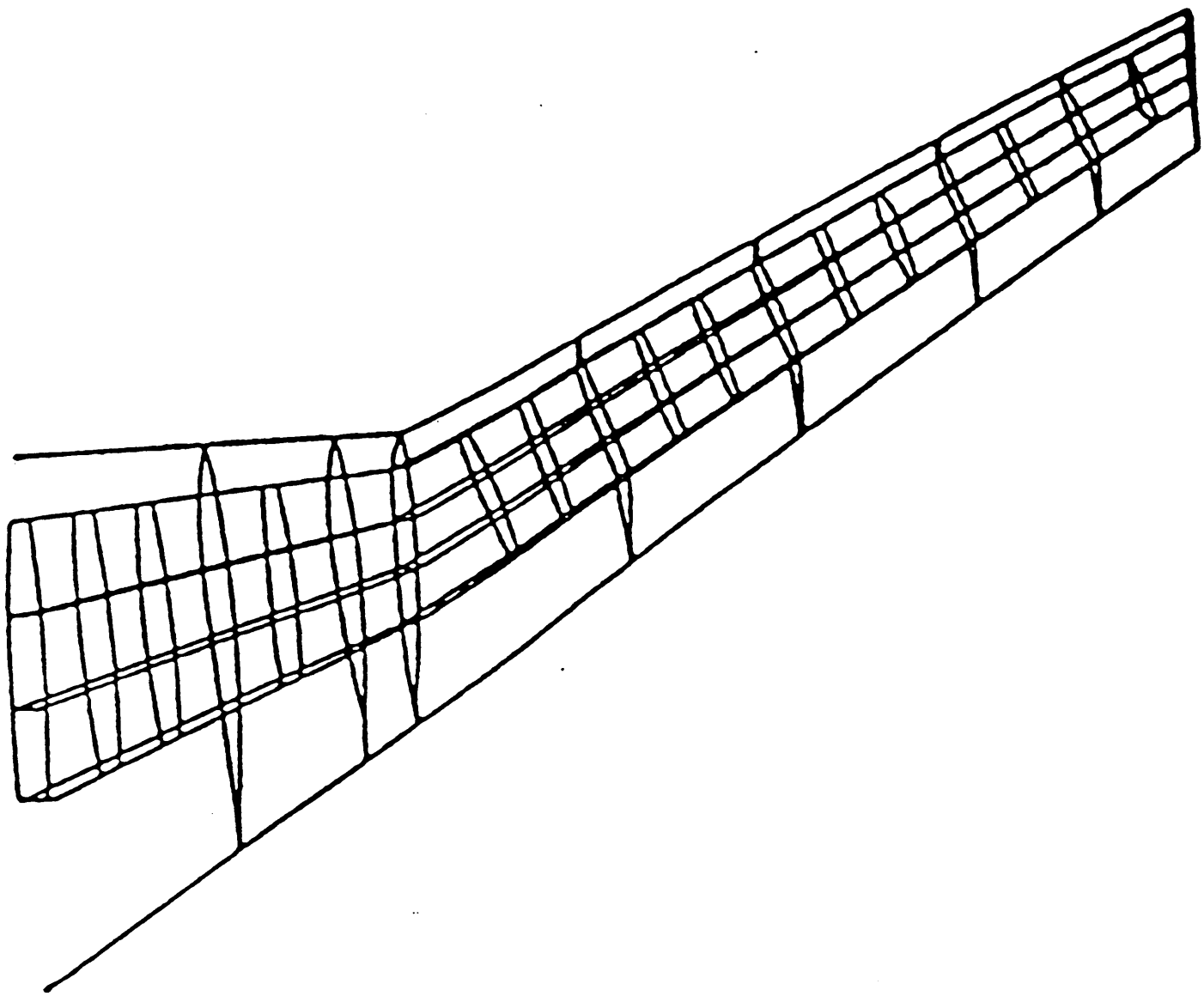

Figure 3. Structural Finite Element Model

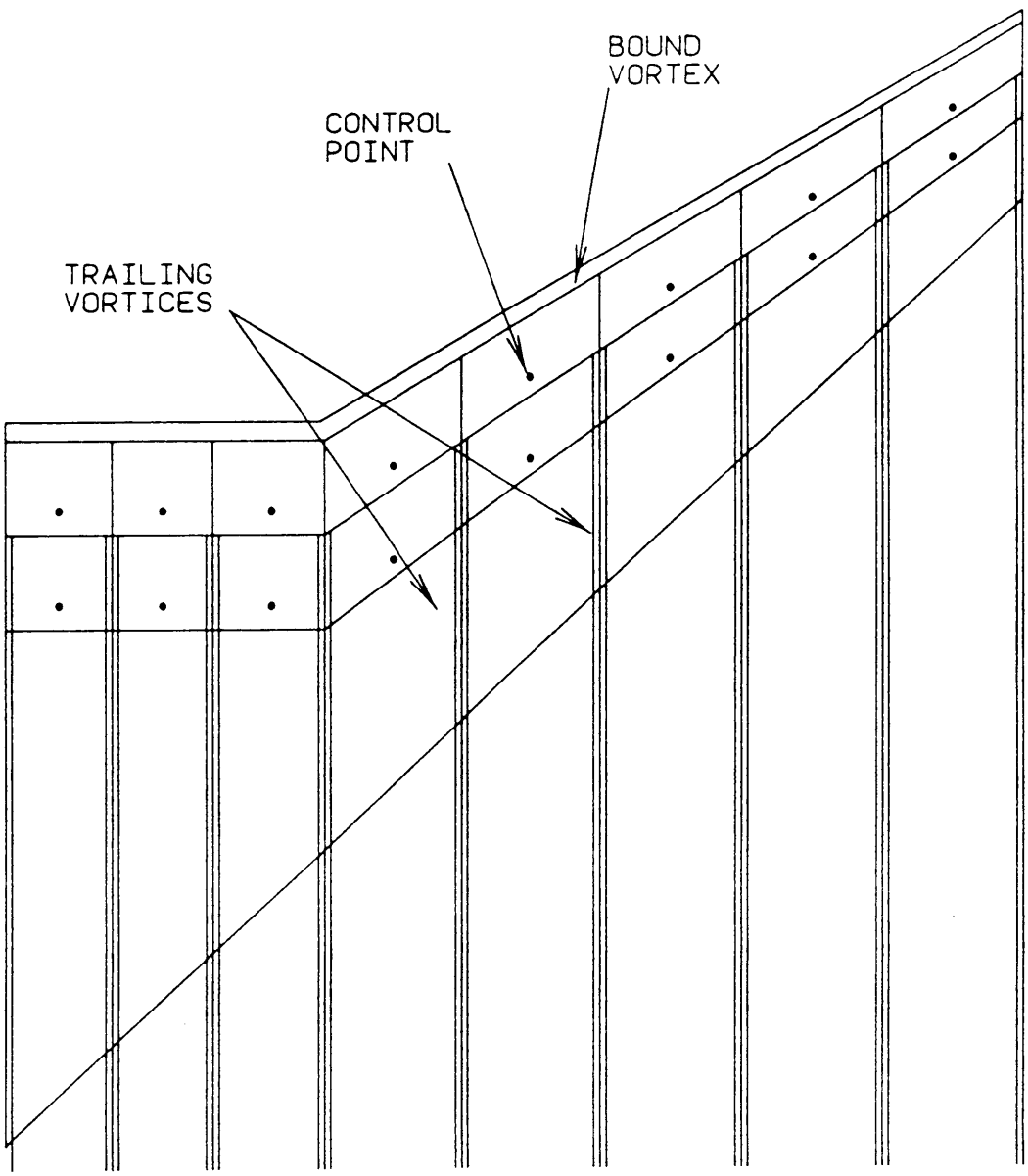

Figure 4. Typical Vortex Lattice Panels and Horseshoe Vortices

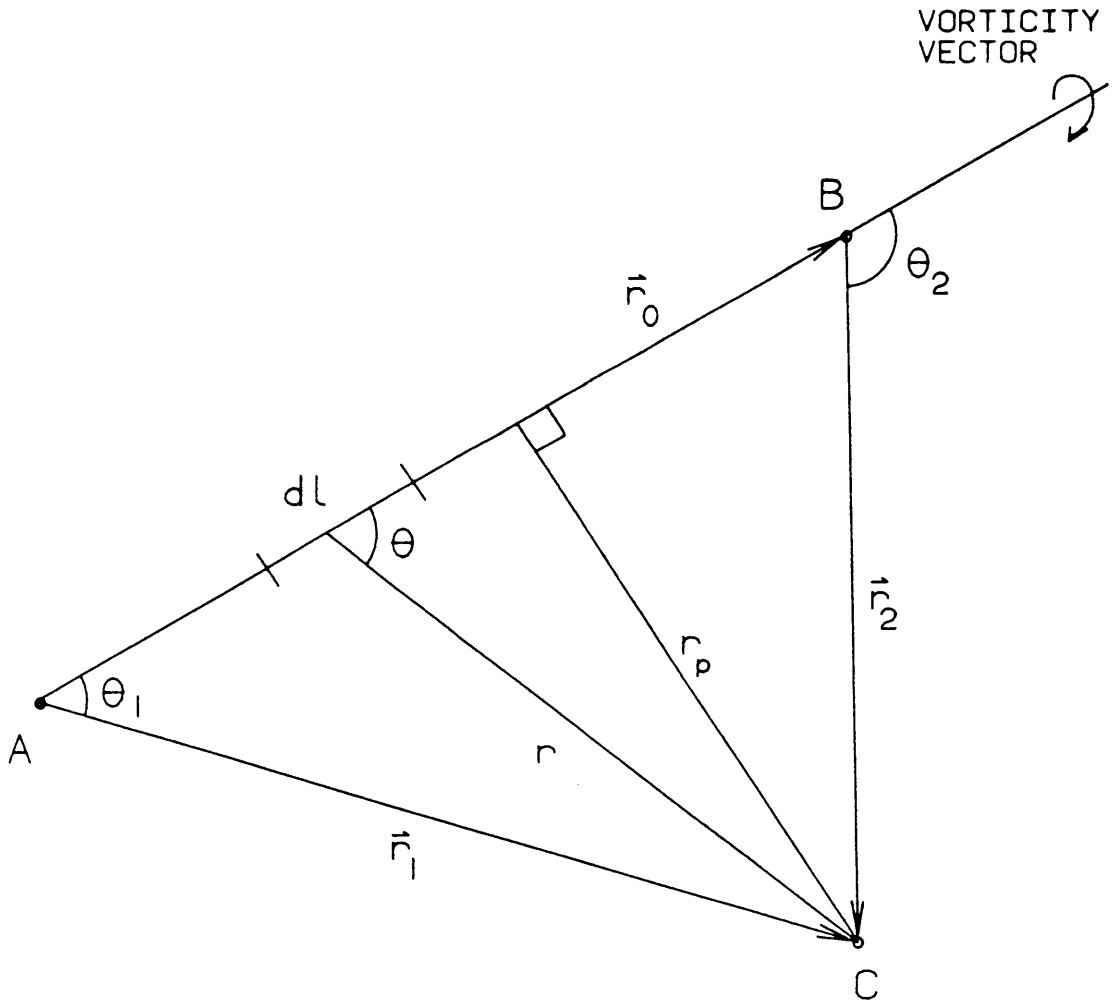

Figure 5. Diagram for Velocity Induced at a Point

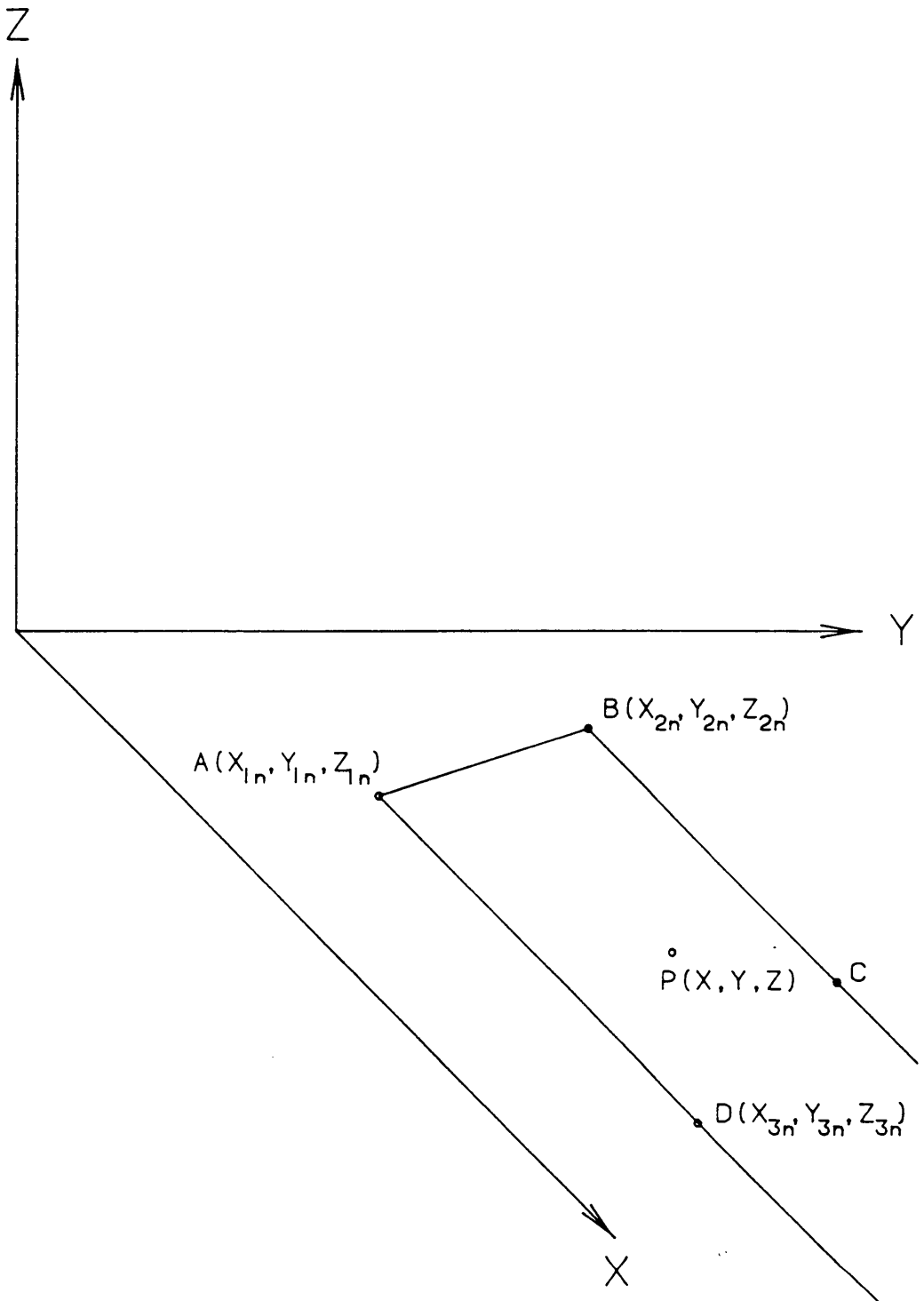

Figure 6. Typical Horseshoe Vortex and Control Point

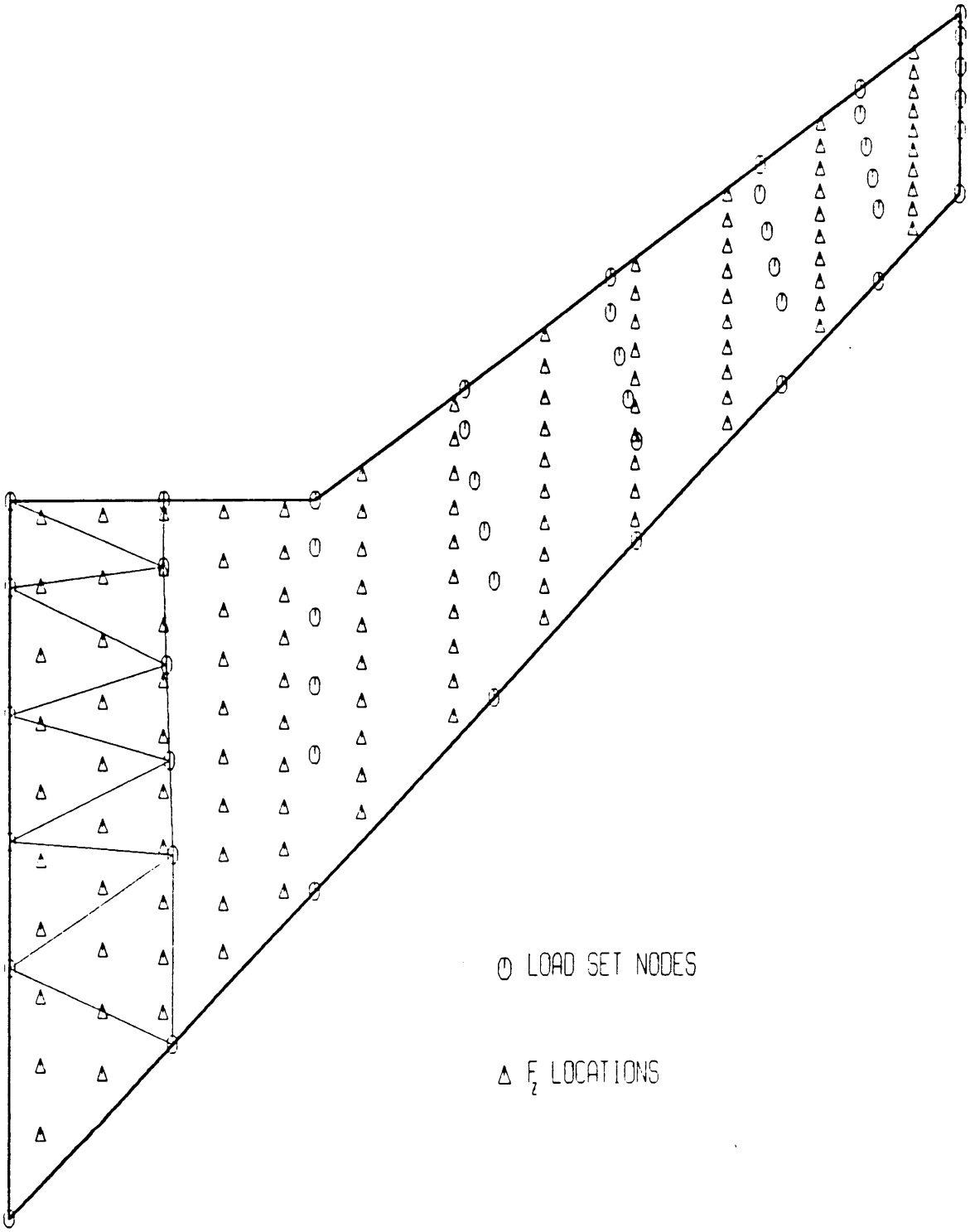

Figure 7. Aerodynamic Force Locations and Load Set Nodes ; Sample Triangular Regions

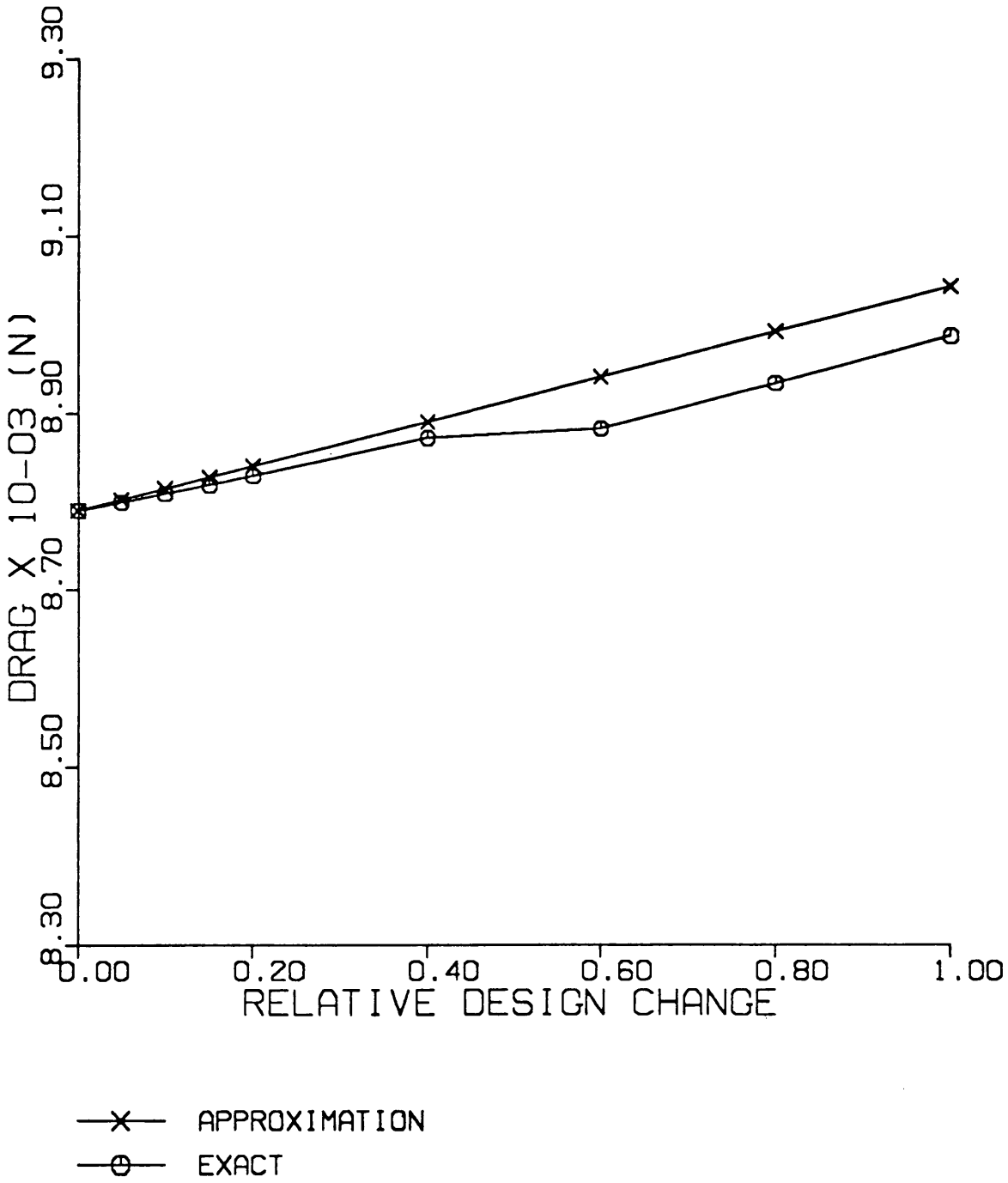

Figure 8. Drag Approximation versus Exact Drag Calculation for One Optimization Cycle

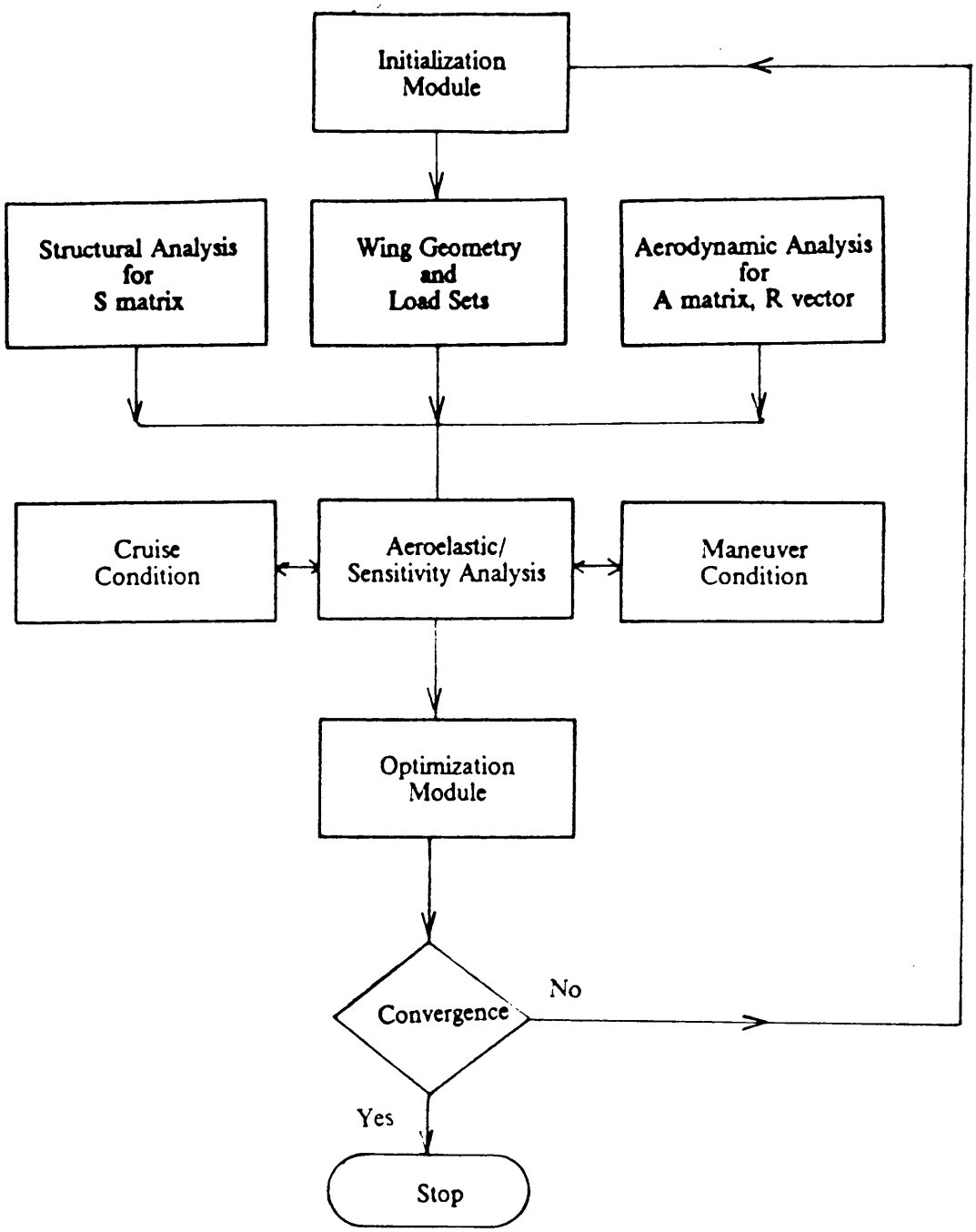

Figure 9. Design Procedure Flowchart

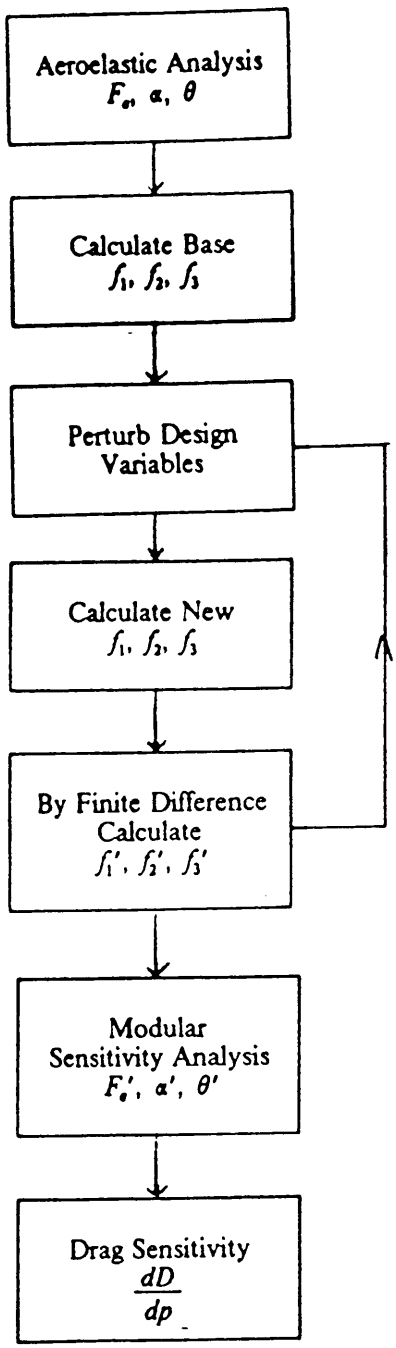

Figure 10. Aeroelastic/Sensitivity Flowchart for Cruise

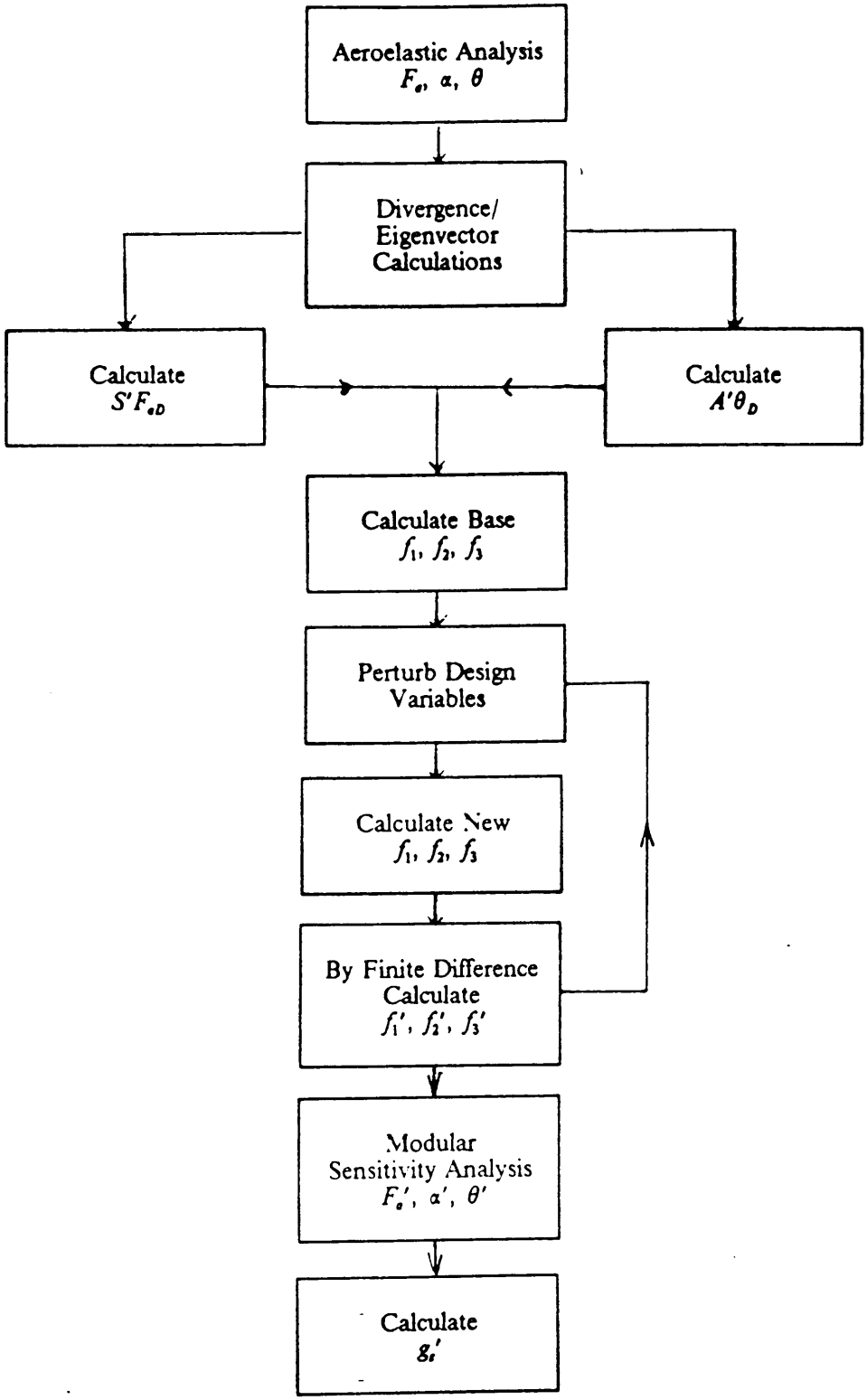

Figure 11. Aeroelastic/Sensitivity Flowchart for Maneuver

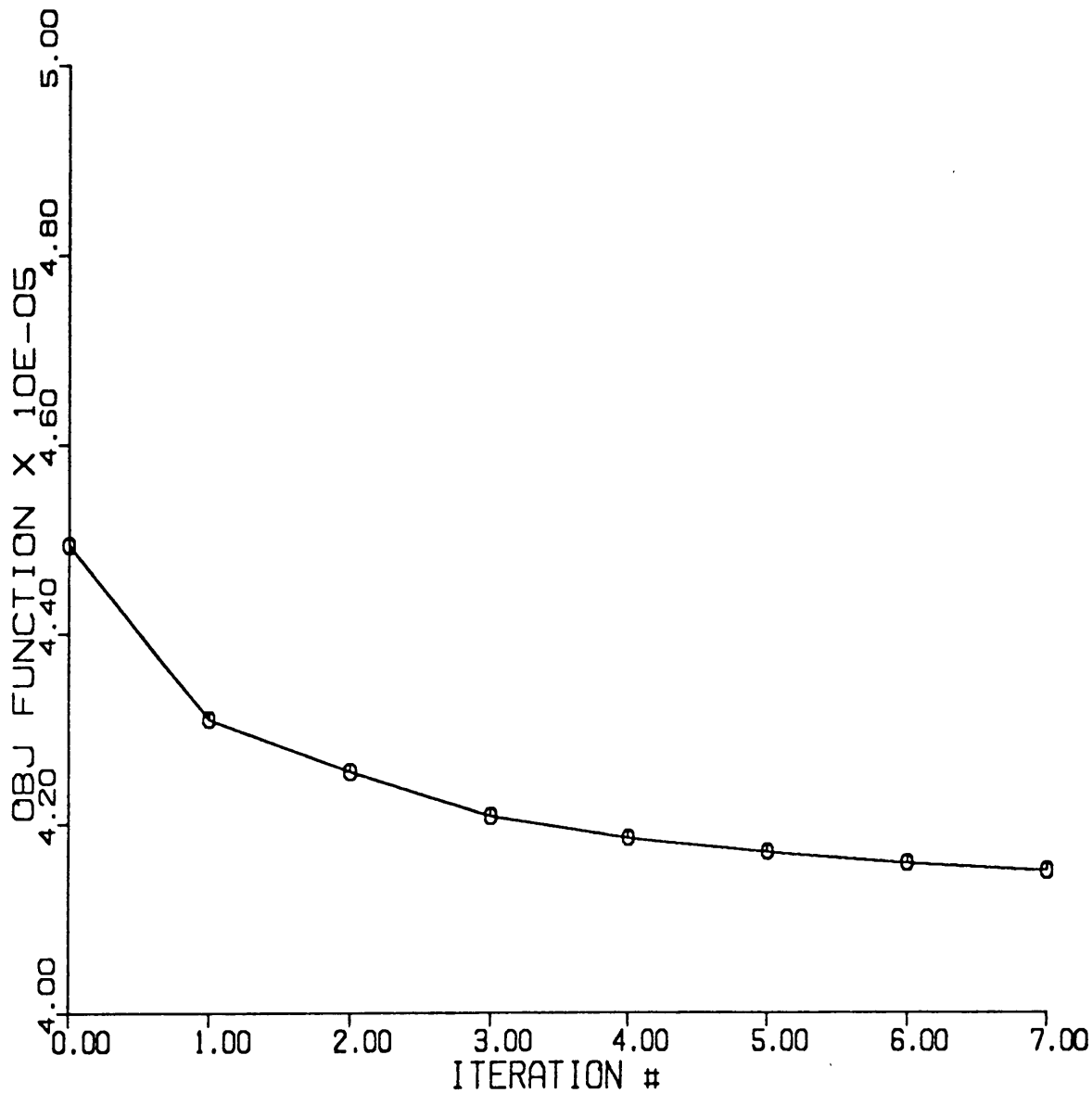

Figure 12. Weight Convergence Plot

The vita has been removed from the scanned document